



1 **Time dependent, non-monotonic response of warm convective cloud fields to**
2 **changes in aerosol loading**

3 **Guy Dagan, Ilan Koren*, Orit Altaratz and Reuven H. Heiblum**

4 Department of Earth and Planetary Sciences, The Weizmann Institute of Science,
5 Rehovot 76100, Israel.

6 * *Correspondence to:* ilan.koren@weizmann.ac.il

7

8 **Abstract**

9 Large Eddy Simulations (LES) with bin microphysics are used here to study cloud
10 fields' sensitivity to changes in aerosol properties and the time evolution of this
11 response. Similarly to the known response of a single cloud, we show that the mean
12 field properties change in a non-monotonic trend, with an optimum aerosol
13 concentration for which the field reaches its maximal water mass or rain yield. This
14 trend is a result of competition between processes that encourage cloud development
15 versus those that suppress it. However, another layer of complexity is added when
16 considering clouds' impact on the field's thermodynamic properties and how this is
17 dependent on aerosol loading. Under polluted conditions rain is suppressed, and the
18 non-precipitating clouds act to increase atmospheric instability. This results in
19 warming of the lower part of the cloudy layer (in which there is net condensation) and
20 cooling of the upper part (net evaporation). Evaporation at the upper part of the
21 cloudy layer in the polluted simulations raises humidity at these levels and thus
22 amplifies the development of the next generation of clouds (preconditioning effect).
23 On the other hand, under clean conditions, the precipitating clouds drive net warming
24 of the cloudy layer and net cooling of the sub-cloud layer due to rain evaporation.
25 These two effects act to stabilize the atmospheric boundary layer with time
26 (consumption of the instability). Evolution of the field's thermodynamic properties
27 affects the cloud properties in return, as shown by migration of the optimal aerosol
28 concentration toward higher values.

29



30 **1. Introduction**

31 Despite the extensive research conducted in the last few decades, and the fact that
32 clouds have an important role in the Earth's energy balance (Trenberth et al., 2009)
33 clouds are still considered to be one of the largest source of uncertainty in the study of
34 climate and climate change (Forster et al., 2007; Boucher et al., 2013).

35 Warm cloud (containing liquid water only) formation depends on the availability of
36 aerosols acting as cloud condensation nuclei (CCN). Changes in aerosol concentration
37 modulate the cloud droplet size distribution and total number. Polluted clouds
38 (forming under high aerosol loading) initially have smaller and more numerous
39 droplets, with narrower size distribution compared to clean clouds (Squires, 1958;
40 Squires and Twomey, 1960; Warner and Twomey, 1967; Fitzgerald and Spyers-
41 Duran, 1973).

42 The initial droplet size distribution affects key cloud processes such as condensation-
43 evaporation, collision-coalescence and sedimentation. The condensation-evaporation
44 process is proportional to the total droplet surface area which increases with the
45 droplet number concentration (for a given total liquid water mass). Under given
46 supersaturation conditions, the condensation in polluted clouds is more efficient
47 (Pinsky et al., 2013; Seiki and Nakajima, 2014; Koren et al., 2014; Kogan and Martin,
48 1994; Dagan et al., 2015a). However, under sub-saturation conditions, due to the same
49 reason, it implies higher evaporation efficiency. The evaporation induces downdrafts
50 and stronger vorticity and hence can lead to stronger mixing of the cloud with its
51 environment in polluted conditions (Xue and Feingold, 2006; Jiang et al., 2006; Small
52 et al., 2009).

53 The initiation of collision-coalescence is delayed in polluted clouds (Gunn and
54 Phillips, 1957; Squires, 1958; Albrecht, 1989). This drives a delay in rain formation
55 and can affect the amount of surface rain (Rosenfeld, 1999, 2000; Koren et al., 2012;
56 Khain, 2009; Levin and Cotton, 2009; Dagan et al., 2015b).

57 Aerosol effects on single warm convective clouds were shown to have an optimal
58 value with respect to maximal water mass, cloud depth and rain yield (Dagan et al.,
59 2015a,b). For aerosol concentrations lower than the optimum, the positive relationship
60 between aerosol concentration and cloud development is a result of two main



61 processes: 1) larger latent heat release driven by the increase in the condensation
62 efficiency causing stronger updrafts, and 2) decrease in the effective terminal velocity
63 (η , i.e. mass weighted terminal velocity of the hydrometeors), (Koren et al., 2015) due
64 to initial smaller droplets and the delay in the collision-coalescence process. The
65 smaller droplets have higher mobility (the water mass moves up better with
66 surrounding updraft), reaching higher in the atmosphere and prolonging the cloud
67 growth.

68 For aerosol concentration values above the optimum, the suppressing aerosol effects
69 take over, namely: 1) stronger mixing of the cloud with its environment driven by the
70 increased evaporation efficiency (Small et al., 2009), and 2) increased water loading
71 effect due to the rain suppression.

72 Understanding of the overall aerosol effect is even more complex when considering
73 processes on the cloud field scale. Clouds affect the surrounding thermodynamic
74 conditions by changing the humidity and temperature profiles (Lee et al., 2014;
75 Seifert et al., 2015; Stevens and Feingold, 2009; Saleeby et al., 2015). In addition,
76 clouds affect the solar and longwave radiation budgets in the field. Over land the
77 radiation effects change the surface temperature and therefore can significantly affect
78 heat and moist fluxes, and as a result the cloud properties (Koren et al., 2004, 2008;
79 Feingold et al., 2005).

80 The invigoration mechanism, which refers to larger clouds with larger mass that
81 develop under polluted conditions was studied mainly in deep convective clouds
82 (Andreae et al., 2004; Koren et al., 2005; Rosenfeld et al., 2008; Tao et al., 2012; Fan
83 et al., 2013; Altaratz et al., 2014). Our focus here is on warm cloud fields for which
84 previous observational studies reported on invigoration effect or a non-monotonic
85 response of the clouds to an increase in aerosol loading. For example, Kaufman et al.,
86 (2005) found an increase in cloud fraction (CF) of warm cloud fields with increasing
87 aerosol loading over the tropical Atlantic Ocean. Yuan et al. (2011) reported that an
88 increase in volcanic aerosols near Hawaii led to increased trade cumulus CF and
89 clouds top height. Dey et al. (2011) have shown that an increase in aerosol optical
90 depth (AOD) from clean to slightly polluted resulted in an increase in CF in warm
91 clouds over the Indian Ocean. Additional increase in the AOD resulted in a decrease
92 of CF, explained by the semi direct effect of absorbing aerosols. Costantino and Bréon



93 (2013) reported higher CF over the south-eastern Atlantic under high aerosol loading
94 conditions. Koren et al. (2014) have shown that warm convective clouds over the
95 Southern Oceans can be considered as aerosol limited up to moderate aerosol loading
96 conditions. As the AOD increases, the clouds were shown to be larger and to produce
97 stronger rain rates. A reversal in trend of liquid water path (LWP) as a function of
98 increasing AOD was reported using observations of warm convective clouds under
99 large range of meteorological conditions (Savane et al., 2015). Li et al. (2011) studied
100 warm clouds over the southern great plains of the United States and reported no
101 aerosol effect on clouds' top height.

102 On the other hand, numerical studies of the aerosol's effect on warm cumulus cloud
103 fields show either no effect or cloud suppression (meaning shallower and smaller
104 clouds under higher aerosol loading conditions). Jiang and Feingold (2006) found that
105 the LWP, CF, and cloud depth of warm shallow convective clouds are insensitive to
106 an increase in aerosol loading. However, they did demonstrate rain suppression by
107 aerosols. Xue et al. (2008) showed smaller clouds and suppression of precipitation in
108 increased aerosol loading environment. Jiang et al. (2010) found a non-monotonic
109 change in the derivative of the surface rain rate with aerosol loading (susceptibility)
110 for higher maximal LWP clouds, but a monotonic decrease in the total precipitation
111 with aerosol loading. Seigel (2014) showed that the clouds' size decreases with
112 aerosol loading due to enhanced entrainment at clouds' margins.

113 Some previous studies have demonstrated clouds alteration of their environment
114 (Zhao and Austin, 2005; Heus and Jonker, 2008; Malkus, 1954; Lee et al., 2014;
115 Zuidema et al., 2012; Roesner et al., 1990). One example of such effect is the
116 "preconditioning" or "cloud deepening" effect (Nitta and Esbensen, 1974; Roesner et
117 al., 1990; Stevens, 2007; Stevens and Seifert, 2008), where clouds cool and moisten
118 the upper cloudy and inversion layers and by that encourage the development of the
119 next generation of clouds that encounter improved environmental conditions. This
120 effect is influenced by the clouds' microphysical properties (Stevens and Feingold,
121 2009; Saleeby et al., 2015). The role of warm convective clouds in moistening of the
122 free troposphere was studied intensively using both observations and cloud field
123 numerical models (Brown and Zhang, 1997; Johnson et al., 1999; Takemi et al., 2004;
124 Kuang and Bretherton, 2006; Holloway and Neelin, 2009; Waite and Khouider,
125 2010).



126 Albrecht (1993) used a theoretical single column model to study the effect of
127 precipitation on the thermodynamic structure of trade wind boundary layer and found
128 that even low rain rates can dramatically affect the profiles. Under precipitating
129 conditions, the cloud layer is warmer, drier, and more stable than under non-
130 precipitation conditions. He also showed that under non-precipitating conditions the
131 inversion height is greater than under precipitating conditions, due to the larger
132 amount of liquid water evaporated at those elevations.

133 Another way clouds effect their environment is by evaporation of rain below the cloud
134 base which induces cooling of the sub-cloudy layer (Zuidema et al., 2012; Heiblum et
135 al., 2016a). Lee et al. (2014) demonstrated the aerosol effects on the field's CAPE (as
136 distributed above cloud base or below it). The organization of the field is influenced
137 by cloud processes as well. Enhanced evaporative cooling in the sub-cloud layer, for
138 example, can produce cold pools which enhance the generation of clouds only at their
139 boundaries, and hence change the organization of the field (Seigel, 2014; Seifert and
140 Heus, 2013; Heiblum et al., 2016a).

141 A recent paper (Dagan et al., 2016) showed that polluted clouds act to increase the
142 thermodynamic instability with time, while clean clouds consume the atmospheric
143 instability. The trend of the pollution driven increase in the instability is halted once
144 the clouds are thick enough to develop significant precipitation. Indeed, studies of
145 long simulation times (>30 hr), showed that the initial differences between clean and
146 polluted cases are reduced by negative feedbacks of the clouds on the thermodynamic
147 conditions (Lee et al., 2012; Seifert et al., 2015).

148 In this work we explore the coupled microphysical-dynamic system of warm marine
149 cloud fields. We studied how changes in aerosol concentrations affect cloud
150 properties and the related modifications of the environmental thermodynamic
151 conditions over time.

152

153 **2. Methodology**

154 The SAM (System for Atmospheric Modeling), non-hydrostatic, anelastic LES model
155 version 6.10.3 (Khairoutdinov and Randall, 2003) was used to simulate the well-
156 studied trade cumulus case of BOMEX (Holland and Rasmusson, 1973; Siebesma et
157 al., 2003). The BOMEX case is an idealized trade-cumulus cloud field that is based on



158 observations made near Barbados during June 1969. This case was initialized using
159 the setup specified in (Siebesma et al., 2003). The setup includes surface fluxes and
160 large scale forcing (see details in Heiblum et al., 2016b). The horizontal resolution
161 was set to 100 m while the vertical resolution was set to 40 m. The domain size was
162 $12.8 \times 12.8 \times 4.0 \text{ km}^3$ and the time step was 1 sec. Due to computational limitations,
163 we had to restrict the domain size to a scale that has a limited capacity for capturing
164 large scale organization (Seifert and Heus, 2013). The model ran for sixteen hours and
165 the statistical analysis included all but the first two hours (total of 14 hours).

166 A bin microphysical scheme (Khain and Pokrovsky, 2004) was used. The scheme
167 solves warm microphysical processes, including droplet nucleation, diffusional
168 growth, collision coalescence, sedimentation and breakup.

169 The aerosol distribution was based on measurements of marine aerosol size
170 distribution (see details in Jaenicke 1988 and Altaratz et al., 2008). Eight different
171 simulations were conducted with a changing aerosol concentration (5, 25, 50, 100,
172 250, 500, 2000 and 5000 cm^{-3}) (Dagan et al., 2015a).

173

174

175 **3. Results and discussion**

176 **3.1 Mean cloud field properties under different aerosol loading conditions**

177 The aerosol effects on the mean properties of the eight simulated cloud fields are
178 examined first. Figure 1 presents mean values of key properties of cloud fields as a
179 function of the aerosol loading for the entire (14 h) simulation time.

180 The total water mass (calculated as mean over time in each domain) as a function of
181 aerosol concentration shows a clear reversal in the trend (Fig. 1A). It increases when
182 increasing aerosol loading from 5 to 50 cm^{-3} . Additional increase in the aerosol
183 loading results in a decrease in the total water mass in the domain.

184 The LWP (Liquid Water Path - Fig. 1B) calculated as a mean over time over all
185 cloudy columns in each domain, (which is strongly correlated with the total water
186 mass), also shows the same non-monotonic general trend. The maximum in the curve
187 of cloudy LWP is at slightly higher aerosol concentration compared to the total mass
188 (100 cm^{-3}). This difference can be explained by the link to the cloud fraction (CF –
189 calculated as the area covered by clouds with optical path $\tau > 0.3$ Fig. 1C) that
190 decreases above aerosol loading of 25 cm^{-3} . And so, for the more polluted simulations



191 the mass is distributed on smaller horizontal cloud areas as shown in previous studies
192 (Seigel, 2014).

193

194 There is also a significant difference in the way the water mass is distributed along the
195 atmospheric column in the different simulations. The maximum cloud top height (Fig.
196 1D), calculated as a mean over time of the altitude of the highest grid box in the
197 domain that contains liquid water content ($LWC > 0.01 \text{ g/kg}$) increases significantly
198 when increasing aerosol loading up to 500 cm^{-3} (increase from 1692 m to 2120 m
199 when increasing aerosol loading from 5 to 500 cm^{-3}). Additional increase in the
200 aerosol loading results in a minor decrease in the maximum cloud top height (down to
201 2030 m for aerosol loading of 5000 cm^{-3}). The minor decrease seen for this range of
202 aerosol concentration (compared with the larger decrease in the mean LWP for
203 example) can be explained by the location of the maximal cloud top height above the
204 cloud core, which is affected mainly by the invigoration processes (enhanced
205 condensation and latent heat release) and less by margin oriented processes (enhanced
206 entrainment and evaporation) that significantly impact the total cloud mass (Dagan et
207 al., 2015a). Another reason is the cloud deepening effect under polluted conditions
208 (Stevens, 2007; Seifert et al., 2015) that will be described later. As for the mean cloud
209 top height calculated as a mean of all cloudy columns along the whole run (Fig. 1E),
210 the trend shows a monotonic increase with aerosol loading. The trend is approaching a
211 saturation level for high aerosol concentration values. The mean cloud top value over
212 the simulation is 810 and 1010 m for the simulations with aerosol loading of 5 to 5000
213 cm^{-3} , respectively.

214

215 The trend in the domain's average rain rate, as a function of the aerosol loading (Fig.
216 1F) shows a peak at relatively low aerosol loading (similar to optimal value of the CF)
217 of 25 cm^{-3} .

218

219 Fig. 2 presents the mean vertical profiles of the condensation-evaporation tendencies,
220 for four different simulations. We note that as the aerosol loading increases, both the
221 mean condensation and evaporation rates increase (Dagan et al., 2015a; Koren et al.,
222 2014; Pinsky et al., 2013; Seiki and Nakajima, 2014). Below cloud base (located



223 around 550 m) the clean simulations have small rain evaporation values which is
224 absent in the polluted simulations.

225

226 Effective terminal velocity (η) is defined as the mass weighted average terminal
227 velocity of all the hydrometeors within a given volume of air (Koren et al., 2015). By
228 definition, η measures the terminal velocity of the water mass's center of gravity
229 (COG), i.e. the COG's movement with respect to the surrounding air's vertical
230 velocity (W). Small absolute values $|\eta|$ imply that the droplets COG will move better
231 with the surrounding air, i.e. the droplets will have better mobility (Koren et al.,
232 2015). The sum $V_{COG} = W + \eta$ (η always negative) reflects the water mass COG
233 vertical velocity relative to the surface. Positive V_{COG} implies a rise of the COG, and
234 negative value means falling.

235 The mean updraft (in both space and time, weighted by the liquid water mass in each
236 grid box to be consistent with the COG point of view - Fig. 3A) increases with the
237 increase in aerosol loading, in agreement with previous studies (Saleeby et al., 2015;
238 Seigel, 2014). This indicates an increase in the latent heat contribution to the cloud
239 buoyancy, driven by increase in the condensation efficiency (Dagan et al., 2015a,b;
240 Koren et al., 2014; Pinsky et al., 2013; Seiki and Nakajima, 2014) (Fig. 2). At the
241 same time, $|\eta|$ decreases as the aerosol concentration increases (Fig. 3B) indicating
242 better mobility of the smaller droplets, allowing them to move more easily with the
243 air's updrafts. The outcome of these two effects is an increased V_{COG} for higher
244 aerosol concentration (Fig. 3C) indicating that the polluted clouds' liquid water is
245 pushed higher in the atmosphere (Koren et al., 2015) as shown by higher COG (Fig.
246 3D).

247

248 The mean COG height of the water mass (Grabowski et al., 2006; Koren et al., 2009)
249 (Fig. 3D), increases with the aerosol loading up to a relatively high concentration (500
250 cm^{-3}). Note that while the trend in the system's characteristic velocities (η and W) is
251 monotonic increase, the COG has an optimal aerosol concentration for which it
252 reaches its maximum height (500 cm^{-3}). For aerosol concentrations above 500 cm^{-3} a
253 minor decrease is shown. As described above, the COG height increase with aerosol



254 loading, between extremely clean and polluted conditions, can be explained by
255 increased V_{COG} , which is a product of both lower $|\eta|$ and increased updraft in the
256 cloud scale, and larger thermodynamic instability induced by the polluted clouds in
257 the field scale as will be shown in the next section (Dagan et al., 2016; Heiblum et al.,
258 2016a). The reduction of the mean COG height in the most polluted simulations is
259 caused by cloud suppressing processes including an enhanced entrainment (see the
260 enhanced evaporation efficiency with aerosol loading – Fig. 2) and larger water
261 loading (Dagan et al., 2015a - shown also in Fig. 4 below).

262 The trend in COG height can be also viewed (in more detail) in Fig. 4 that presents
263 profiles of mean LWC.

264 We show that both the height and the magnitude of the maximum LWC increase with
265 the aerosol loading. Below the clouds' base ($H < \sim 550\text{m}$) the LWC trend is reversed
266 due to the enhancement of rain in the clean runs (Fig. 1F). The increase in LWC with
267 aerosol loading implies a larger water loading negative component in the clouds'
268 buoyancy.

269

270 All the evidence presented in Figs. 2-4 explains the non-monotonic trends of the
271 clouds properties response to changes in aerosol loading (Fig. 1). For clean conditions
272 (below the optimal aerosol concentration value), an increase in aerosol loading would
273 enhance the cloud development (larger mass, LWP, cloud top, CF, rain rate) because
274 of two main factors: 1) an increase in the condensation efficiency (due to the larger
275 total droplet surface area for condensation and longer time- Fig. 2), and 2) smaller
276 effective terminal velocity (η) values, that per given updraft allow the cloud's
277 hydrometeors to be pushed higher in the atmosphere (Koren et al., 2015) (Fig. 3B).

278 The higher condensation efficiency in polluted clouds (Fig. 2) results in a larger latent
279 heat release that enhances the updraft (Fig. 3A) and cloud development. The increased
280 V_{COG} reflects the two cloud enhancing processes (decrease in $|\eta|$ and larger mean
281 updraft). We note that the increase in the mean updraft values with aerosol loading is
282 seen despite the negative effect of water loading (see Fig. 4). For aerosol
283 concentrations above the optimum, cloud development is suppressed by the increase
284 in evaporation efficiency (Fig. 2) and hence stronger mixing of the cloud with its



285 environment (i.e. Small et al., 2009), and larger water loading due to rain suppression
286 (Dagan et al., 2015a, Fig. 4).

287

288

289 **3.2 The time evolution of the mean cloud field properties under different aerosol** 290 **loading conditions**

291 All the aerosol effects that were discussed up to this point (condensation-evaporation
292 efficiencies, η and water loading) are applicable both on the single cloud scale as well
293 as on the cloud field scale. However, on the cloud field scale, another aspect needs to
294 be considered, namely the time evolution of the effect of clouds on the field's
295 thermodynamic conditions.

296 Figure 5 presents the changes (final value less initial one) in the temperature (T) and
297 water vapor content (q_v) vertical profiles as a function of aerosol concentration used in
298 the simulation. The initial profiles were identical in all simulations. In low aerosol
299 concentration runs (100 cm^{-3} and below) the sub-cloud layer becomes cooler and
300 wetter with time and the cloudy layer warmer and drier. Meanwhile, under higher
301 aerosol concentrations conditions (250 cm^{-3} and above) the sub-cloud layer becomes
302 warmer and drier while the cloudy and inversion layers become colder and wetter.
303 This trend is driven by the condensation-evaporation tendencies along the vertical
304 profile (see Fig. 2, Dagan et al., 2016). Under low aerosol concentration conditions,
305 water condenses at the cloudy layer and is advected downward to the sub-cloud layer
306 where it partially evaporates. Under polluted conditions, on the other hand, the
307 condensed water from the lower part of the cloudy layer is advected up to the upper
308 cloudy and inversion layers (driven by larger V_{COG} - Fig. 3) and evaporates there
309 (Dagan et al., 2016).

310

311 Such trends in the environmental thermodynamic conditions are likely to affect the
312 forming clouds. In Fig. 6 the time evolution of some of the key cloud field properties
313 are considered (the same properties that were shown in Fig. 1). The blue, green and
314 red curves represent the mean values over the first, second and third periods of the
315 simulations, respectively (each one covers 4 hours and 40 min). Table 1 presents



316 change (in percentage) in the mean values of key variables between the third period of
317 the 8 simulations (during the 11:20-16:00 hours of simulation, red curves in Fig. 6)
318 and the first period (02:00-06:40 hours of simulation, blue curves in Fig. 6).

319 Examination of the evolution in the mean total water mass along the simulations (Fig.
320 6A blue, green and red curves) presents a different trend between the clean and the
321 polluted simulations. In the clean simulations ($5\text{-}100\text{ cm}^{-3}$) the total water mass
322 decreases significantly with time (a decrease of 57, 45, 44, 20% in the total mass for
323 the cases of 5, 25, 50 and 100 cm^{-3} respectively – see table 1). On the other hand, in
324 the more polluted simulations, (with aerosol loading of 250 and 500 cm^{-3}) there is an
325 increase in the total water mass with time (of 17 and 37% between the first and the
326 last third periods of the simulations, respectively). Under extreme polluted conditions
327 of 2000 and 5000 cm^{-3} , the total water mass in the domain is small and there is little
328 change with time. These changes in time push the optimum aerosol concentration to
329 higher values along the simulation time. This trend is also shown for the optimum
330 aerosol concentration with regard to the mean cloudy LWP (Fig. 6B), max top (Fig.
331 6D) and mean top (Fig. 6E).

332 Trends in the mean rain rate show that in the cleanest simulations (5, 25 and 50 cm^{-3})
333 it decreases with time (Fig. 1H, 53.3, 32.9 and 40.1%, respectively). In the regime of
334 medium to fairly high aerosol loading (100, 250 and 500 cm^{-3}) the rain rate increases
335 (19.6, 598.1 and 841.5%, respectively). And in the most polluted simulations (2000
336 and 5000 cm^{-3}) the surface rain is negligible throughout the simulation time.
337

338 The time evolution of the thermodynamic conditions (Fig. 5) shows a reduction
339 (enhancement) in the thermodynamic instability with time in the clean (polluted)
340 simulations. Figure 6 and table 1 indicate that under clean conditions the decrease in
341 the thermodynamic instability with time leads to a decrease in the mean cloud field
342 properties such as total mass and cloud top height. Under polluted conditions the
343 trends are opposite and the mean cloud field properties increase with time due to the
344 increase in thermodynamic instability (Dagan et al., 2016) and due to the cloud
345 deepening (Stevens and Seifert, 2008; Stevens, 2007; Seifert et al., 2015). These
346 differences between the clean and polluted simulations drive changes in the optimum
347 aerosol concentration with time. For example, for the LWP (Fig. 1B) the optimum



348 aerosol concentration is 50, 100 and 250 cm⁻³ for the first, second and third parts of
349 the simulation, respectively.

350

351

352 **Summary**

353 Cloud processes can be divided in a simplistic manner into two characteristic scales –
354 the cloud scale and the field scale. Here using LES model with bin microphysical
355 scheme we studied the outcome of the two scales' processes acting together. We first
356 presented domain averaged properties over the whole simulation time (section 3.1) to
357 indicate the general aerosol effects in a first order manner and then we followed the
358 time evolution of the effects (section 3.2).

359 A non-monotonic aerosol effect was reported recently for a single cloud scale (Dagan
360 et al., 2015a,b). Here we show that these trends “survived” the domain and time
361 averaging. We argue that the enhanced development branch trend is driven by two
362 main processes of enhanced condensation and reduced effective terminal velocity
363 (which improves the droplets mobility). These processes are mainly related to the core
364 of the clouds and to the early stages of clouds development. We show that the cloud's
365 systems characteristic velocities can capture these effects. The effective terminal
366 velocity (η) inversely measures the mobility. Smaller droplets with smaller variance
367 will have smaller η and therefore will be pushed higher in a given updraft, whereas
368 larger droplets with larger η will deviate downward faster from the surrounding air.
369 Increase in condensation efficiency drives more latent heat release that enhances the
370 cloud updraft. We showed that V_{COG} is a product of the two velocities.

371 The descending branch in which increase of aerosol loading suppresses cloud
372 development is governed by increase in the evaporation efficiency on the subsaturated
373 parts of the clouds and by increase in water loading.

374 Since clouds change the atmospheric thermodynamic conditions in which they form,
375 different initial clouds would cause different impact on the environment. Therefore,
376 cloud field is a continuously evolving system for which aerosol properties determine
377 an important part of the temporal trends. Figure 5 shows striking differences between
378 the evolution of the thermodynamic profiles in clean and polluted cases. For the
379 polluted clouds (mostly non-precipitating), the upper cloudy layer turns wetter and



380 cooler due to enhanced evaporation and the sub-cloudy layer becomes warmer and
381 drier, which altogether act to increase the instability. On the other hand, clean
382 precipitating clouds consume the initial instability with time by warming the cloudy
383 layer (due to latent heat release) and cooling the sub-cloud layer by evaporation of
384 rain.

385 The polluted cloud feedbacks on the thermodynamic conditions act to deepen the
386 clouds. Since clouds that form in a more unstable environment are expected to be
387 aerosol limited up to higher aerosol concentrations (Koren et al., 2014; Dagan et al.,
388 2015a), an increase in the domains instability for the polluted cases drives an increase
389 in the optimal aerosol concentration with time.

390 We note that such an increase in the instability cannot last forever. A deepened cloud
391 will eventually produce larger precipitation rates that may weaken the overall effect
392 on the field (Stevens and Feingold, 2009; Seifert et al., 2015). These results pose an
393 interesting question on the dynamical state of cloud fields in nature. Do the cloud
394 fields ‘manage’ to reach a “near-equilibrium” state (Seifert et al., 2015), for which the
395 deepening effect balances the aerosol effect fast enough that the effects are buffered
396 most of the time (Stevens and Feingold, 2009). Or maybe, the characteristic lifetime
397 of a trade cumulus cloud field is shorter than the time it takes to significantly balance
398 the aerosol effects. In this case the cloud fields could be regarded as ‘transient’ and
399 therefore, as shown here, aerosol might have a strong effect on the clouds, both
400 through affecting the microphysics, initiating many feedbacks in the cloud scale, and
401 by affecting the field thermodynamic evolution over time.

402

403 **Acknowledgements**

404 This research has been supported by the Minerva foundation with funding from the
405 Federal German Ministry of Education and Research.

406

407 **References**

- 408 Albrecht, B. A.: Aerosols, cloud microphysics, and fractional cloudiness, Science (New York,
409 NY), 245, 1227, 1989.
410 Albrecht, B. A.: Effects of precipitation on the thermodynamic structure of the trade wind
411 boundary layer, Journal of Geophysical Research: Atmospheres (1984–2012), 98,
412 7327-7337, 1993.



- 413 Altaratz, O., Koren, I., Reisin, T., Kostinski, A., Feingold, G., Levin, Z., and Yin, Y.:
 414 Aerosols' influence on the interplay between condensation, evaporation and rain in
 415 warm cumulus cloud, *Atmospheric Chemistry and Physics*, 8, 15-24, 2008.
- 416 Altaratz, O., Koren, I., Remer, L., and Hirsch, E.: Review: Cloud invigoration by aerosols—
 417 Coupling between microphysics and dynamics, *Atmospheric Research*, 140, 38-60,
 418 2014.
- 419 Andreae, M. O., Rosenfeld, D., Artaxo, P., Costa, A. A., Frank, G. P., Longo, K. M., and
 420 Silva-Dias, M. A. F.: Smoking rain clouds over the Amazon, *Science*, 303, 1337-
 421 1342, 10.1126/science.1092779, 2004.
- 422 Boucher, O., Randall, D., Artaxo, P., Bretherton, C., Feingold, G., Forster, P., Kerminen, V.,
 423 Kondo, Y., Liao, H., and Lohmann, U.: Clouds and aerosols, *Climate Change*, 571-
 424 657, 2013.
- 425 Brown, R. G., and Zhang, C.: Variability of midtropospheric moisture and its effect on cloud-
 426 top height distribution during TOGA COARE*, *Journal of the atmospheric sciences*,
 427 54, 2760-2774, 1997.
- 428 Costantino, L., and Bréon, F.-M.: Aerosol indirect effect on warm clouds over South-East
 429 Atlantic, from co-located MODIS and CALIPSO observations, *Atmospheric*
 430 *Chemistry and Physics*, 13, 69-88, 2013.
- 431 Dagan, G., Koren, I., and Altaratz, O.: Competition between core and periphery-based
 432 processes in warm convective clouds—from invigoration to suppression, *Atmospheric*
 433 *Chemistry and Physics*, 15, 2749-2760, 2015a.
- 434 Dagan, G., Koren, I., and Altaratz, O.: Aerosol effects on the timing of warm rain processes,
 435 *Geophysical Research Letters*, 42, 4590-4598, 10.1002/2015GL063839, 2015b.
- 436 Dagan, G., Koren, I., Altaratz, O., and Heiblum, R. H.: Aerosol effect on the evolution of the
 437 thermodynamic properties of warm convective cloud fields, *Scientific Reports*, in
 438 review, 2016.
- 439 Dey, S., Di Girolamo, L., Zhao, G., Jones, A. L., and McFarquhar, G. M.: Satellite-observed
 440 relationships between aerosol and trade-wind cumulus cloud properties over the
 441 Indian Ocean, *Geophysical Research Letters*, 38, 2011.
- 442 Fan, J., Leung, L. R., Rosenfeld, D., Chen, Q., Li, Z., Zhang, J., and Yan, H.: Microphysical
 443 effects determine macrophysical response for aerosol impacts on deep convective
 444 clouds, *Proceedings of the National Academy of Sciences*, 110, E4581-E4590, 2013.
- 445 Feingold, G., Jiang, H. L., and Harrington, J. Y.: On smoke suppression of clouds in
 446 Amazonia, *Geophysical Research Letters*, 32, 10.1029/2004gl021369, 2005.
- 447 Fitzgerald, J., and Spyers-Duran, P.: Changes in cloud nucleus concentration and cloud
 448 droplet size distribution associated with pollution from St. Louis, *Journal of Applied*
 449 *Meteorology*, 12, 511-516, 1973.
- 450 Forster, P., Ramaswamy, V., Artaxo, P., Berntsen, T., Betts, R., Fahey, D. W., Haywood, J.,
 451 Lean, J., Lowe, D. C., Myhre, G., Nganga, J., Prinn, R., Raga, G., Schulz, M., and
 452 Dorland, R. V.: Changes in Atmospheric Constituents and in Radiative Forcing., in:
 453 *Climate Change 2007: The Physical Science Basis. Contribution of Working Group I*
 454 *to the Fourth Assessment Report of the Intergovernmental Panel on Climate Change*,
 455 edited by: Solomon, S., D. Qin, M. Manning, Z. Chen, M. Marquis, K.B. Averyt,
 456 M.Tignor and H.L. Miller Cambridge University Press, Cambridge, United Kingdom
 457 and New York, NY, USA., 2007.
- 458 Grabowski, W., Bechtold, P., Cheng, A., Forbes, R., Halliwell, C., Khairoutdinov, M., Lang,
 459 S., Nasuno, T., Petch, J., and Tao, W. K.: Daytime convective development over land:
 460 A model intercomparison based on LBA observations, *Quarterly Journal of the Royal*
 461 *Meteorological Society*, 132, 317-344, 2006.
- 462 Gunn, R., and Phillips, B.: An experimental investigation of the effect of air pollution on the
 463 initiation of rain, *Journal of Meteorology*, 14, 272-280, 1957.
- 464 Heiblum, R. H., Altaratz, O., Koren, I., Feingold, G., Kostinski, A. B., Khain, A. P.,
 465 Ovchinnikov, M., Fredj, E., Dagan, G., and Pinto, L.: Characterization of cumulus
 466 cloud fields using trajectories in the center-of-gravity vs. water mass phase space.



- 467 Part II: Aerosol effects on warm convective clouds, *Journal of Geophysical Research:*
 468 *Atmospheres*, 2016a.
- 469 Heiblum, R. H., Altaratz, O., Koren, I., Feingold, G., Kostinski, A. B., Khain, A. P.,
 470 Ovchinnikov, M., Fredj, E., Dagan, G., and Pinto, L.: Characterization of cumulus
 471 cloud fields using trajectories in the center of gravity versus water mass phase space:
 472 1. Cloud tracking and phase space description, *Journal of Geophysical Research:*
 473 *Atmospheres*, 2016b.
- 474 Heus, T., and Jonker, H. J.: Subsiding shells around shallow cumulus clouds, *Journal of the*
 475 *Atmospheric Sciences*, 65, 1003-1018, 2008.
- 476 Holland, J. Z., and Rasmusson, E. M.: Measurements of the atmospheric mass, energy, and
 477 momentum budgets over a 500-kilometer square of tropical ocean, *Monthly Weather*
 478 *Review*, 101, 44-55, 1973.
- 479 Holloway, C. E., and Neelin, J. D.: Moisture vertical structure, column water vapor, and
 480 tropical deep convection, *Journal of the atmospheric sciences*, 66, 1665-1683, 2009.
- 481 Jaenicke, R.: Aerosol physics and chemistry, *Landolt-Börnstein Neue Serie 4b*, 391-457,
 482 1988.
- 483 Jiang, H., Xue, H., Teller, A., Feingold, G., and Levin, Z.: Aerosol effects on the lifetime of
 484 shallow cumulus, *Geophysical Research Letters*, 33, 10.1029/2006gl026024, 2006.
- 485 Jiang, H., Feingold, G., and Sorooshian, A.: Effect of aerosol on the susceptibility and
 486 efficiency of precipitation in warm trade cumulus clouds, *Journal of the Atmospheric*
 487 *Sciences*, 67, 3525-3540, 2010.
- 488 Jiang, H. L., and Feingold, G.: Effect of aerosol on warm convective clouds: Aerosol-cloud-
 489 surface flux feedbacks in a new coupled large eddy model, *Journal of Geophysical*
 490 *Research-Atmospheres*, 111, D01202 10.1029/2005jd006138, 2006.
- 491 Johnson, R. H., Rickenbach, T. M., Rutledge, S. A., Ciesielski, P. E., and Schubert, W. H.:
 492 Trimodal characteristics of tropical convection, *Journal of climate*, 12, 2397-2418,
 493 1999.
- 494 Kaufman, Y. J., Koren, I., Remer, L. A., Rosenfeld, D., and Rudich, Y.: The effect of smoke,
 495 dust, and pollution aerosol on shallow cloud development over the Atlantic Ocean,
 496 *Proceedings of the National Academy of Sciences of the United States of America*,
 497 102, 11207-11212, 10.1073/pnas.0505191102, 2005.
- 498 Khain, A., and Pokrovsky, A.: Simulation of effects of atmospheric aerosols on deep turbulent
 499 convective clouds using a spectral microphysics mixed-phase cumulus cloud model.
 500 Part II: Sensitivity study, *Journal of the Atmospheric Sciences*, 61, 2983-3001,
 501 10.1175/jas-3281.1, 2004.
- 502 Khain, A. P.: Notes on state-of-the-art investigations of aerosol effects on precipitation: a
 503 critical review, *Environmental Research Letters*, 4, 015004 (015020 pp.)-015004
 504 (015020 pp.), 10.1088/1748-9326/4/1/015004, 2009.
- 505 Khairoutdinov, M. F., and Randall, D. A.: Cloud resolving modeling of the ARM summer
 506 1997 IOP: Model formulation, results, uncertainties, and sensitivities, *Journal of the*
 507 *Atmospheric Sciences*, 60, 2003.
- 508 Kogan, Y. L., and Martin, W. J.: Parameterization of bulk condensation in numerical cloud
 509 models, *Journal of the atmospheric sciences*, 51, 1728-1739, 1994.
- 510 Koren, I., Kaufman, Y. J., Remer, L. A., and Martins, J. V.: Measurement of the effect of
 511 Amazon smoke on inhibition of cloud formation, *Science*, 303, 1342-1345,
 512 10.1126/science.1089424, 2004.
- 513 Koren, I., Kaufman, Y. J., Rosenfeld, D., Remer, L. A., and Rudich, Y.: Aerosol invigoration
 514 and restructuring of Atlantic convective clouds, *Geophysical Research Letters*, 32,
 515 10.1029/2005gl023187, 2005.
- 516 Koren, I., Martins, J. V., Remer, L. A., and Afargan, H.: Smoke invigoration versus inhibition
 517 of clouds over the Amazon, *Science*, 321, 946-949, 10.1126/science.1159185, 2008.
- 518 Koren, I., Altaratz, O., Feingold, G., Levin, Z., and Reisin, T.: Cloud's Center of Gravity - a
 519 compact approach to analyze convective cloud development, *Atmospheric Chemistry*
 520 *and Physics*, 9, 155-161, 2009.



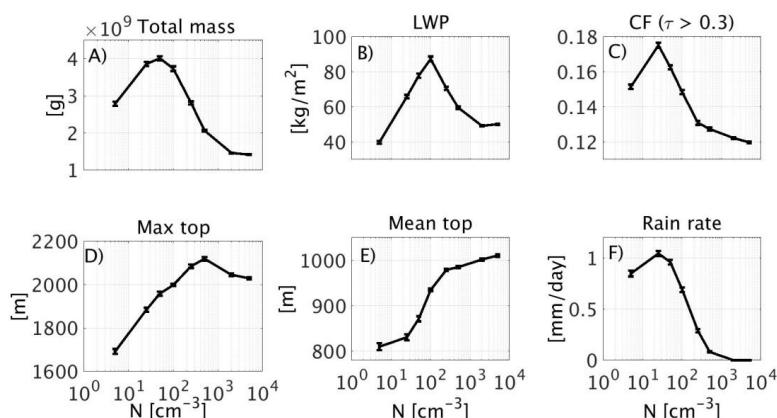
- 521 Koren, I., Altaratz, O., Remer, L. A., Feingold, G., Martins, J. V., and Heiblum, R. H.:
522 Aerosol-induced intensification of rain from the tropics to the mid-latitudes, *Nature*
523 *Geoscience*, 2012.
- 524 Koren, I., Dagan, G., and Altaratz, O.: From aerosol-limited to invigoration of warm
525 convective clouds, *science*, 344, 1143-1146, 2014.
- 526 Koren, I., Altaratz, O., and Dagan, G.: Aerosol effect on the mobility of cloud droplets,
527 *Environmental Research Letters*, 10, 104011, 2015.
- 528 Kuang, Z., and Bretherton, C. S.: A mass-flux scheme view of a high-resolution simulation of
529 a transition from shallow to deep cumulus convection, *Journal of the Atmospheric*
530 *Sciences*, 63, 1895-1909, 2006.
- 531 Lee, S.-S., Feingold, G., and Chuang, P. Y.: Effect of aerosol on cloud–environment
532 interactions in trade cumulus, *Journal of the Atmospheric Sciences*, 69, 3607-3632,
533 2012.
- 534 Lee, S. S., Kim, B.-G., Lee, C., Yum, S. S., and Posselt, D.: Effect of aerosol pollution on
535 clouds and its dependence on precipitation intensity, *Climate Dynamics*, 42, 557-577,
536 2014.
- 537 Levin, Z., and Cotton, W. R.: *Aerosol pollution impact on precipitation: A scientific review*,
538 Springer, 2009.
- 539 Li, Z., Niu, F., Fan, J., Liu, Y., Rosenfeld, D., and Ding, Y.: Long-term impacts of aerosols on
540 the vertical development of clouds and precipitation, *Nature Geoscience*, 4, 888-894,
541 10.1038/ngeo1313, 2011.
- 542 Nitta, T., and Esbensen, S.: Heat and moisture budget analyses using BOMEX data, *Monthly*
543 *Weather Review*, 102, 17-28, 1974.
- 544 Pinsky, M., Mazin, I., Korolev, A., and Khain, A.: Supersaturation and diffusional droplet
545 growth in liquid clouds, *Journal of the Atmospheric Sciences*, 70, 2778-2793, 2013.
- 546 Roesner, S., Flossmann, A., and Pruppacher, H.: The effect on the evolution of the drop
547 spectrum in clouds of the preconditioning of air by successive convective elements,
548 *Quarterly Journal of the Royal Meteorological Society*, 116, 1389-1403, 1990.
- 549 Rosenfeld, D.: TRMM observed first direct evidence of smoke from forest fires inhibiting
550 rainfall, *Geophysical Research Letters*, 26, 3105-3108, 10.1029/1999gl006066, 1999.
- 551 Rosenfeld, D.: Suppression of rain and snow by urban and industrial air pollution, *Science*,
552 287, 1793-1796, 10.1126/science.287.5459.1793, 2000.
- 553 Rosenfeld, D., Lohmann, U., Raga, G. B., O'Dowd, C. D., Kulmala, M., Fuzzi, S., Reissell,
554 A., and Andreae, M. O.: Flood or drought: How do aerosols affect precipitation?,
555 *Science*, 321, 1309-1313, 10.1126/science.1160606, 2008.
- 556 Saleeby, S. M., Herbener, S. R., van den Heever, S. C., and L'Ecuyer, T.: Impacts of Cloud
557 Droplet–Nucleating Aerosols on Shallow Tropical Convection, *Journal of the*
558 *Atmospheric Sciences*, 72, 1369-1385, 2015.
- 559 Savane, O. S., Vant-Hull, B., Mahani, S., and Khanbilvardi, R.: Effects of Aerosol on Cloud
560 Liquid Water Path: Statistical Method a Potential Source for Divergence in Past
561 Observation Based Correlative Studies, *Atmosphere*, 6, 273-298, 2015.
- 562 Seifert, A., and Heus, T.: Large-eddy simulation of organized precipitating trade wind
563 cumulus clouds, *Atmos. Chem. Phys.*, 13, 5631-5645, 2013.
- 564 Seifert, A., Heus, T., Pincus, R., and Stevens, B.: Large-eddy simulation of the transient and
565 near-equilibrium behavior of precipitating shallow convection, *Journal of Advances*
566 *in Modeling Earth Systems*, 2015.
- 567 Seigel, R. B.: Shallow Cumulus Mixing and Subcloud Layer Responses to Variations in
568 Aerosol Loading, *Journal of the Atmospheric Sciences*, 2014.
- 569 Seiki, T., and Nakajima, T.: Aerosol effects of the condensation process on a convective
570 cloud simulation, *Journal of the Atmospheric Sciences*, 71, 833-853, 2014.
- 571 Siebesma, A. P., Bretherton, C. S., Brown, A., Chlond, A., Cuxart, J., Duynkerke, P. G.,
572 Jiang, H., Khairoutdinov, M., Lewellen, D., and Moeng, C. H.: A large eddy
573 simulation intercomparison study of shallow cumulus convection, *Journal of the*
574 *Atmospheric Sciences*, 60, 1201-1219, 2003.



- 575 Small, J. D., Chuang, P. Y., Feingold, G., and Jiang, H.: Can aerosol decrease cloud lifetime?,
576 Geophysical Research Letters, 36, 2009.
- 577 Squires, P.: The microstructure and colloidal stability of warm clouds, *Tellus*, 10, 262-271,
578 1958.
- 579 Squires, P., and Twomey, S.: The relation between cloud droplet spectra and the spectrum of
580 cloud nuclei, *Geophysical Monograph Series*, 5, 211-219, 1960.
- 581 Starr Malkus, J.: Some results of a trade-cumulus cloud investigation, *Journal of*
582 *Meteorology*, 11, 220-237, 1954.
- 583 Stevens, B.: On the growth of layers of nonprecipitating cumulus convection, *Journal of the*
584 *atmospheric sciences*, 64, 2916-2931, 2007.
- 585 Stevens, B., and Seifert, R.: Understanding macrophysical outcomes of microphysical choices
586 in simulations of shallow cumulus convection, *Journal of the Meteorological Society*
587 *of Japan*, 86, 143-162, 2008.
- 588 Stevens, B., and Feingold, G.: Untangling aerosol effects on clouds and precipitation in a
589 buffered system, *Nature*, 461, 607-613, 10.1038/nature08281, 2009.
- 590 Takemi, T., Hirayama, O., and Liu, C.: Factors responsible for the vertical development of
591 tropical oceanic cumulus convection, *Geophysical research letters*, 31, 2004.
- 592 Tao, W.-K., Chen, J.-P., Li, Z., Wang, C., and Zhang, C.: Impact of aerosols on convective
593 clouds and precipitation, *Reviews of Geophysics*, 50, RG2001, 2012.
- 594 Trenberth, K. E., Fasullo, J. T., and Kiehl, J.: Earth's global energy budget, *Bull. Amer.*
595 *Meteor. Soc.*, 90, 311-323, 2009.
- 596 Waite, M. L., and Khouider, B.: The deepening of tropical convection by congestus
597 preconditioning, *Journal of the Atmospheric Sciences*, 67, 2601-2615, 2010.
- 598 Warner, J., and Twomey, S.: The production of cloud nuclei by cane fires and the effect on
599 cloud droplet concentration, *Journal of the atmospheric Sciences*, 24, 704-706, 1967.
- 600 Xue, H. W., and Feingold, G.: Large-eddy simulations of trade wind cumuli: Investigation of
601 aerosol indirect effects, *Journal of the Atmospheric Sciences*, 63, 1605-1622,
602 10.1175/jas3706.1, 2006.
- 603 Xue, H. W., Feingold, G., and Stevens, B.: Aerosol effects on clouds, precipitation, and the
604 organization of shallow cumulus convection, *Journal of the Atmospheric Sciences*,
605 65, 392-406, 10.1175/2007jas2428.1, 2008.
- 606 Yuan, T., Remer, L. A., and Yu, H.: Microphysical, macrophysical and radiative signatures of
607 volcanic aerosols in trade wind cumulus observed by the A-Train, *Atmospheric*
608 *Chemistry and Physics*, 11, 7119-7132, 10.5194/acp-11-7119-2011, 2011.
- 609 Zhao, M., and Austin, P. H.: Life cycle of numerically simulated shallow cumulus clouds.
610 Part I: Transport, *Journal of the Atmospheric Sciences*, 62, 1269-1290,
611 10.1175/jas3414.1, 2005.
- 612 Zuidema, P., Li, Z., Hill, R. J., Bariteau, L., Rilling, B., Fairall, C., Brewer, W. A., Albrecht,
613 B., and Hare, J.: On trade wind cumulus cold pools, *Journal of the Atmospheric*
614 *Sciences*, 69, 258-280, 2012.

615

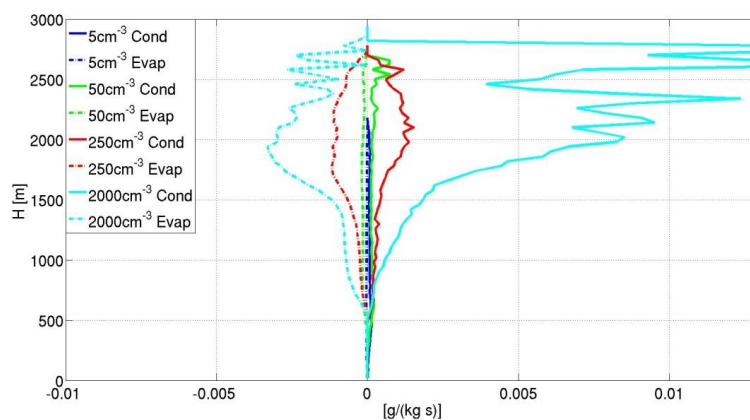
616



617

618 **Figure 1.** mean properties (over domain and time) of the simulated cloud fields as a function of
619 the aerosol concentration used in the simulation: A) total liquid water mass in the domain, B)
620 cloudy LWP, C) cloud fraction (CF) for columns with $\tau > 0.3$, D) maximum cloud top, E) mean
621 cloud top, and, F) surface rain rate. Each of these mean properties are calculated for the last 14
622 hours out of the 16 hours of simulation. The error bars present the standard errors. For details
623 about the different properties see the text.

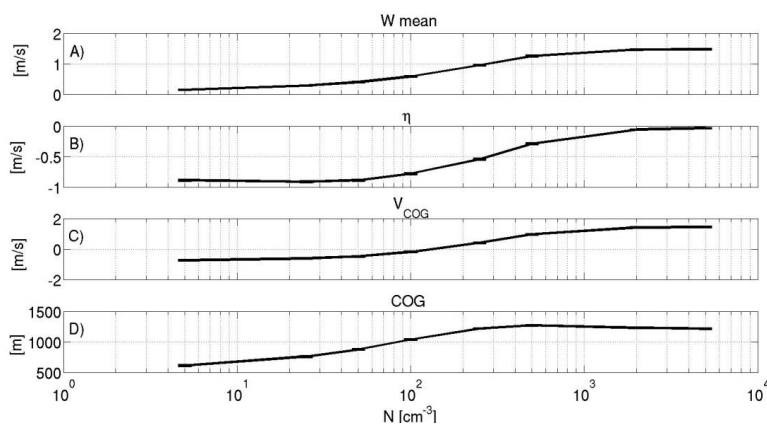
624



625

626 **Figure 2.** Domain mean condensation (solid lines) and evaporation (dashed lines) tendencies for
627 four different simulations conducted with different aerosol concentration levels (5 cm^{-3} blue, 50
628 cm^{-3} green, 250 cm^{-3} red and 2000 cm^{-3} cyan).

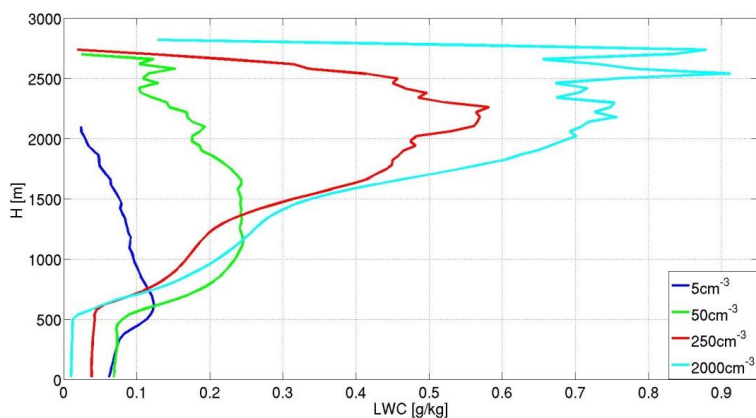
629



630

631 **Figure 3.** Mean (over time and space) of **A) updraft (W), B) effective terminal velocity (η), C) the**
632 **center of gravity velocity V_{COG} and D) COG (center of gravity) height as a function of the aerosol**
633 **concentration. All calculated for the last 14 hours out of the 16 hours of simulation.**

634



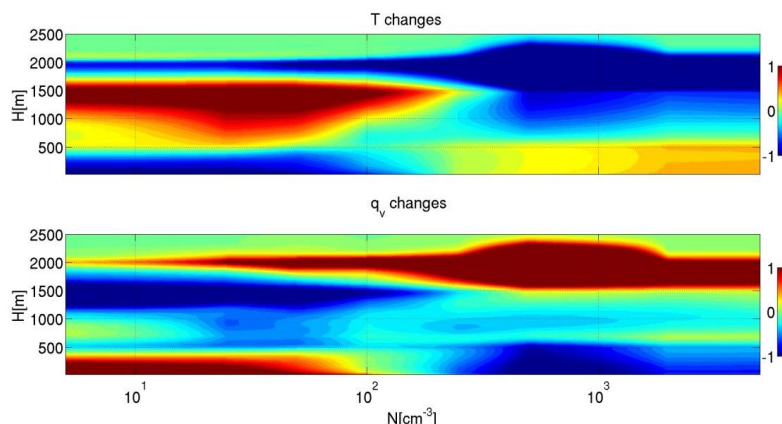
635

636 **Figure 4.** Mean liquid water content (LWC) vertical profiles for four different simulations (5 cm^{-3}

637 **blue, 50 cm^{-3} green, 250 cm^{-3} red and 2000 cm^{-3} cyan). The mean profiles are calculated for the**

638 **last 14 hours out of the 16 hours of simulation.**

639

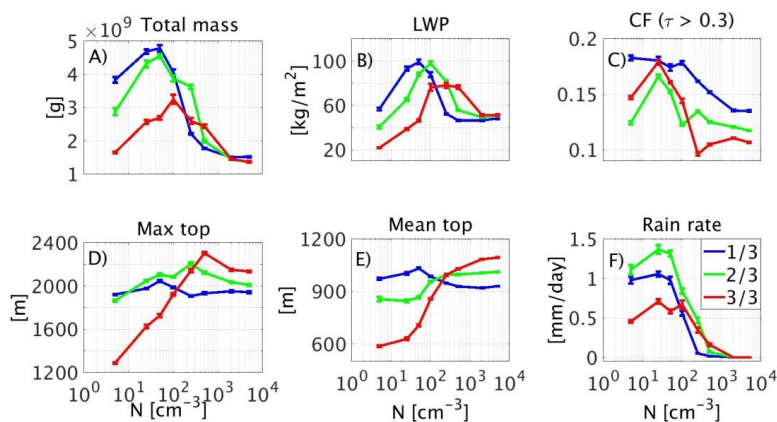


640

641 **Figure 5.** Total change, during 16 h of simulation in the temperature ([k] upper panel) and water
 642 vapor content ([g/kg] – lower panel) domain mean vertical profiles as a function of the aerosol
 643 concentration used in the simulation.

644

645



646

647 **Figure 6.** Mean properties (over time and domain) of the simulated cloud fields as a function of
 648 the aerosol concentration used in the simulation: A) total liquid water mass in the domain, B)
 649 cloudy LWP, C) cloud fraction (CF) for columns with $\tau > 0.3$, D) maximum cloud top, E) mean
 650 cloud top, and, F) surface rain rate. Each property is calculated separately for each period of one
 651 third of the simulations (blue, green and red for the first, second and third periods, respectively).
 652 The error bars present the standard error. For details about the different properties, see the
 653 text.

654



655 **Table 1. change (in %) in key variables between the mean values in the last third period of the**
 656 **simulations and the first period. Negative values are presented in red.**

	Total mass [%]	LWP [%]	COG [%]	Max top [%]	Mean top [%]	W max [%]	CF [%]	Rain rate [%]
5 cm ⁻³	-57.0	-61.4	-43.1	-32.9	-39.7	-28.2	-19.7	-53.5
25 cm ⁻³	-45.2	-58.3	-39.6	-17.8	-37.4	-38.8	-0.6	-32.9
50 cm ⁻³	-43.8	-53.1	-33.7	-15.6	-31.6	-47.9	-7.5	-40.1
100 cm ⁻³	-20.1	-13.0	-16.1	-3.2	-13.0	-32.8	-19.0	19.6
250 cm ⁻³	17.5	48.6	5.0	12.4	5.0	-4.3	-40.7	598.1
500 cm ⁻³	37.4	64.2	19.9	19.2	10.7	9.4	-30.9	841.5
2000 cm ⁻³	-3.7	10.6	14.8	10.1	17.9	6.0	-17.8	-
5000 cm ⁻³	-10.1	5.7	13.7	9.9	17.5	2.9	-20.7	-

657

658